

Improved methods for mapped grids: Applied to highly excited vibrational states of diatomic molecules

S. Kallush*, R. Kosloff

The Fritz Haber Research Center, The Hebrew University of Jerusalem, Jerusalem 91904, Israel

Received 22 October 2006; in final form 7 November 2006

Available online 16 November 2006

Abstract

The origin of an artifact known as the appearance of *ghost states* in mapped Fourier grid methods is investigated. It was found that the ghost states can be attributed to under sampling of the high momentum components which are folded from the inner to the outer region of the potential to create the ghosts. The effect was corrected by addition of a complex potential at the outer region. The exterior complex potential was shown to shift the ghost states to the continuum part of the spectrum in a controllable way. The various methods to improve the mapped grid method are discussed in this context, and the use of zero boundary conditions is shown to be not essential. © 2006 Elsevier B.V. All rights reserved.

1. Introduction

The computational cost of a quantum calculation crucially depends on the size of the Hilbert space N used for the simulation. Dynamical calculations can be made to scale semi linearly with the number N ($O(N \log N)$) directly for propagation methods, or as $O(N^3)$ for methods based on diagonalization [1]. Practically, N becomes the number of grid points required to converge the calculation. Efficient computational methods tend to minimize the number N as much as possible. The idea is to limit the representation to points where the probability amplitude of the wavefunction is above a certain threshold value. A pre-estimation of the number of grid points can be obtained by examining the representation boundaries in phase space. Once an upper limit for the energy in the calculation is established, the phase space volume contained in this energy shell can be calculated from the Hamiltonian. In one dimension the minimum number of points N is the phase space volume \mathcal{V} divided by \hbar , $N_{\min} = \frac{\mathcal{V}}{\hbar}$ [2]. Outside the energy shell the wavefunction will decay exponentially

fast and some sampling points are required to represent the evanescent part of the wavefunction. As a result the actual number of points required to achieve exponential convergence is larger than $N_{\min} = \frac{\mathcal{V}}{\hbar}$ [2,3]. In addition, sampling considerations increase further the number of grid points. For example, a uniform grid has a rectangular shape in phase space. The boundaries of such a grid have to be set to contain the extreme points of the energy shell. If the shape of the energy shell is convoluted most of the phase space area of the rectangular representation is wasted. This leads to a lower sampling efficiency $\eta = \frac{N_{\min}}{N} \ll 1$. The problem is particularly acute in the field of ultracold scattering and photoassociation. A very small grid spacing is required to represent the maximum momentum the colliding atoms acquire when they approach each other. On the other hand, the grid has to be extended to extremely large distances in order to describe the very long De-Broglie wavelength of the cold atoms in free space. The sampling efficiency can be as low as $\eta \approx 10^{-4}$.

A solution to the grid optimization problem was suggested by Fatal et al. [4] which introduced a mapping function from a uniform to a non-uniform grid. Such a grid has a denser sampling at points with higher momentum values. As a result, the sampling correlates position with momentum. An important addition to the mapping procedure

* Corresponding author.

E-mail address: kallush@fh.huji.ac.il (S. Kallush).

was developed by Kokoouline et al. [5] suggesting the use of a semiclassical mapping function. The idea is to relate the local grid spacing to the inverse of the classical momentum corresponding to the value of the energy shell at that point. An improvement of the sampling to account for regions where the semi-classical approximation is not valid was suggested by Nest and Meyer [6]. Since its introduction the semiclassical procedure has been extensively used in the field of ultracold molecules [7]. For example calculating the last bound levels of alkali diatomic molecules as well as in simulating photoassociation of ultracold atom pairs [8,9]. The mapping procedure enabled accurate calculation of these processes which was not possible before.

Despite this success, a troubling artifact appeared and was termed *ghost states* [10]. The signature of these states showed unphysical energy states embedded in the physical spectrum of bound states. Most of the amplitude of the ghost was at large interatomic distances. The exact origin of the ghost states has never been fully understood. It was found that the use of fixed boundary conditions that vanish at the end of the grid eliminate some of the ghost states. This enforcement of zero boundary conditions is restrictive. Moreover, it sets constraints on the number of grid points to contain exact integer number of periods, a limitation which does not necessarily relate directly to the system under consideration.

In this Letter we characterize in more details the ghost states and suggest an explanation of their origin. We show also that a complex scaling of the potential, namely, the addition of imaginary boundary conditions to the potential can be used as a simple and natural solution to the removal of ghost states.

The outline of this Letter is as follows: in Section 2 we will describe shortly the mapped Fourier grid method, following Refs. [5,10]. Section 3 will investigate the features of the ghost states and will try to deduce explanation of their origin. In Section 4 we will show the usefulness of an addition of an exterior complex potential in removing these states from the spectrum. Section 5 will conclude and summarize the discussion.

2. The mapped fourier grid method

The purpose of the mapping procedure is to find the most efficient grid representation for the Hamiltonian of the form:

$$\hat{H} = \hat{T} + \hat{V} \quad (1)$$

where \hat{H} , \hat{T} and \hat{V} are the Hermitian Hamiltonian, kinetic and potential energy operators. A *uniform* Fourier grid will be built according to the following steps:

1. The energy space of the problem E_{\max} and E_{\min} is estimated. Typically E_{\min} is the bottom of the attractive potential and E_{\max} is the maximum kinetic energy of the colliding pair to be represented on the grid.

2. Using E_{\max} and a semiclassical estimation of tunneling R_{\min} is determined. R_{\max} is determined to include all the interval needed to represent the last bound state. The grid interval becomes $L_R = R_{\max} - R_{\min}$.
3. By estimating the maximal kinetic energy $T_{\max} = E_{\max} - V_{\min}$, the maximal possible semiclassical momentum is calculated $p_{\max} = \sqrt{2mT_{\max}}$, where m is the reduced mass of the pair. The corresponding grid in momentum space has to comply with $|p| \leq p_{\max}$, so that $L_p = 2p_{\max}$.
4. Each volume in phase space at the size of \hbar should hold at least one grid point. The number of grid points to support the system will be than given by: $N\hbar = L_R L_p$.
5. Distribute the N grid points equally on the grid (each grid point at the middle of a segment).

The operator \hat{V} in this coordinate representation is diagonal. The kinetic energy operator \hat{T} can be evaluated either numerically by bidirectional FFT, or analytically as :

$$\hat{T}_{i,i} = \frac{\pi^2}{mL_R^2} \frac{N^2 + 2}{6} \quad (2)$$

$$\hat{T}_{i \neq j} = \frac{\pi^2}{mL_R^2} \frac{(-1)^{i-j}}{\sin^2[(i-j)\pi/N]} \quad (3)$$

assuming an even number of grid points. For the case of odd number of points see [11]. For large grids the numerical application of \hat{T} is more efficient since it scales as $O(N \log N)$ compared with $O(N^3)$ for applying Eq. (3) while the accuracy of the two is comparable.

An important feature of the uniform Fourier grid method is that the considerations for choosing the grid are *global*. Each of the grid points can support the largest possible momentum required. This over-estimation is reduced significantly by using a Mapped Fourier Grid. The algorithm for building a mapped Fourier grid is the following:

1. Use the same grid length in coordinates L_R as was determined in the uniform Fourier grid method.
2. Beginning from the inner grid point R_{\min} , integrate the local classical action up to β to get R_1 :

$$\beta = \left(\frac{2m}{\pi^2}\right)^{\frac{1}{2}} \int_{R_{\min}}^{R_1} \sqrt{E_{\text{add}} - V(r)} dr. \quad (4)$$

- E_{add} is given by the maximal asymptotic kinetic energy to be represented on the grid, usually with small additional energy to allow the extension of the grid to classically forbidden zones. The parameter $\beta \leq 1$ serves as an estimation for the local volume coverage in phase space. Smaller values of β will distribute more points on the grid, while for $\beta = 1$ the minimal classical estimation for the needed phase space density of the points is taken.
3. Continue to integrate the action from R_1 to get R_2 , R_3 etc. to the end of the physical grid, with $R_N = R_{\max}$.
 4. The length of the *mapped* grid L_x is given by $\beta(N - 1)$.

The matrix representation of \widehat{V} is still diagonal at the $\{R_n\}, n = 1, \dots, N$ grid points. To represent \widehat{T} one has to calculate the diagonal Jacobian operator for the change of variables from the mapped to the physical grid dR/dx . This is given simply by:

$$\widehat{J}(R_n) = \left. \frac{dR}{dx} \right|_{R_n} = \beta' |_{R_n} = \sqrt{\frac{2m}{\pi^2} [E_{\text{add}} - V(R_n)]} \quad (5)$$

Now the kinetic energy operator is given by the matrix multiplication:

$$\widehat{T} = -\frac{\pi^2}{2mL_x^2} \widehat{J}^{-1/2} \widehat{D} \widehat{J}^{-1} \widehat{D} \widehat{J}^{-1/2} \quad (6)$$

Where \widehat{D} is the first derivative operator, given by:

$$\widehat{D}_{i,j} = \left(\frac{d}{dx} \right)_{i,j} = \begin{cases} 0, & i = j \\ \frac{(-1)^{i-j}}{\sin[(i-j)\pi/N]}, & i \neq j \end{cases} \quad (7)$$

Note that this algorithm eliminates any numerical differentiation which was found to be a source of inaccuracies in [10]. We comment here that the integrand on Eq. (4) $\mathcal{J}^{2\text{nd}} = \sqrt{2m(E_{\text{add}} - V)}/\pi$ originated from a semiclassical approximation for the wavefunction. To incorporate for regions in the potential where the WKB is not valid, one can use the ideas of Ref. [6], and replace $\mathcal{J}^{2\text{nd}}$ by $\mathcal{J}^{3\text{rd}} = 1/\Delta$, where Δ is the (analytical) solution of the equation:

$$|E_{\text{add}} - V|\Delta^2 + \frac{2}{3}|V'|\Delta^3 = \frac{\pi^2}{2m} \quad (8)$$

where V' denotes a derivative of the potential with respect to the position.

In this paper we will make our demonstration by calculating the eigenenergies and eigenstates of the lowest triplet state of the Cesium molecule, $a^3\Sigma_u^+$. The potential surface for this state supports 54 bound states, with a binding energy of $8.91 \times 10^{-6} \text{ cm}^{-1}$ for the most weakly bound state, and spatial extension of ≈ 2500 Bohrs.

3. Ghost states

In a converged grid, when calculating the eigenvalues, each of the calculated eigenfunctions can be associated to a physical stationary state. The mapped grid method may lead to an artifact, a state embedded in the spectrum which has no physical meaning and called a ghost state. Our task is first to identify these states, and then to remove them. For a progression of vibrational states one expects that the adjacent energy intervals $\delta E(v) = E(v) - E(v-1)$ is also a smooth function of v , the vibrational quantum number. Fig. 1 presents the calculated spectrum $-\log(-E(v))$ and the energy intervals $-\log(\delta E(v))$ as a function of the vibrational quantum number v , for a grid size $L_R = 3030$ Bohr, and $\beta = 0.6$. The number of grid points for these parameters is $N = 1258$. A uniform Fourier grid

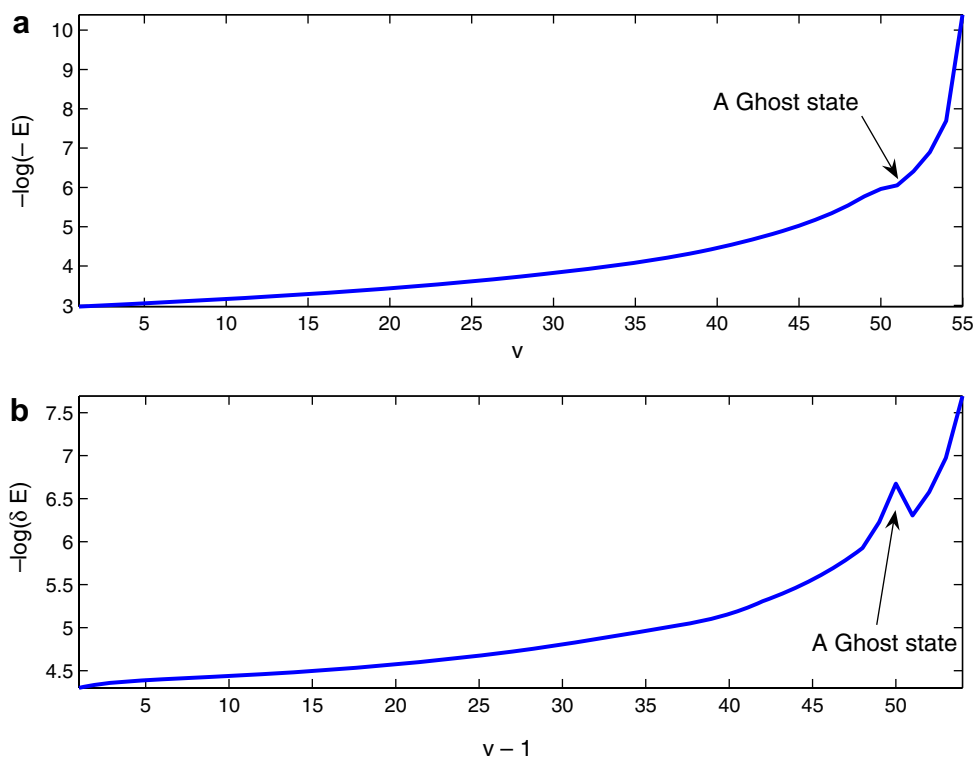


Fig. 1. (a) Vibrational eigenvalues $\log E(v)$ for the bound states of the $a^3\Sigma_u^+$ potential in Cs_2 , as a function of the quantum number v . (b) The energy interval $\log(\delta E(v))$. The eigenenergy corresponds to the ghost is indicated.

for this coverage will demand more than $N = 40\,000$ grid points. The discontinuity that appears at the spectrum close to $v = 51$ is a clear indication of such a ghost state.

Once the ghost state has been identified, we want to understand its character by comparing it to an adjacent physical state. The left panels of Fig. 2 display the wavefunctions of the ghost $v' = 51$ state and the nearby $v = 50$ state. The ghost state can be characterized by an unphysical oscillatory behavior in the classically forbidden region. Both the physical and the ghost states are almost identical in the region where the potential is almost flat, but the small amplitude of these oscillations for the physical state are barely noticeable. This finding indicates that the source of the error is a global representation problem. Further insight regarding the source of the error could be obtained by inspecting the wavefunction in momentum space. The first two panels of Fig. 3 are the momentum space representation $|\bar{\psi}(p)|$ of the two states of Fig. 2. The middle panel shows the expected behavior for a stationary state in momentum space. The number of oscillations of the wavefunction enumerate the quantum number v . This main feature is almost entirely smeared out for the highly excited vibrational state due to the concentration of the probability around zero momentum $p = 0$ with low kinetic energy. The wavefunction of the unphysical state shows fingerprints of a periodic behavior, but it seems like a discrete superposition of several plane waves, and not of a bound state. A change in the grid length, for a constant β , leaves the erroneous eigenenergy and the wavefunction in both position

and momentum space unchanged. The bottom panel of Fig. 3 shows the unphysical wave function in momentum space for $\beta = 0.8$, i.e., a less dense grid in the position space. The eigenenergy of the state is lowered, and becomes $v' = 40$. The characteristic features of the wavefunction remain the same, but the superposition is now over denser plane wave components. For $\beta \leq 0.585$, the ghost state is removed from the bound spectrum.

The combination of these features, indicates that the source of the systematic error is the result of an under sampling of the wavefunction in momentum. In terms of the spectral methods, the sampling is below the Nyquist frequency. A high momentum component in the potential well leaks to the asymptotic region where it is undersampled. As a result it obtains an artificially lower kinetic energy component. An extension of the grid in the position space increases the resolution in momentum space, but leaves the grid increment, and accordingly the ghost state, unchanged. An increase of density of the points, i.e., decrease of β , extends the grid increment in momentum space and allows the support of higher momentum components. As β decreases, the expression of the missed momentum components is given in terms of higher momentum components and its eigenenergy is driven toward the unbound part of the spectrum until it finally disappears.

The problem of undersampling of the potential is more acute at regions where the potential changes rapidly and the semi-classical sampling criterion (Eq. (4)) is no longer valid. The use of \mathcal{J}^{3rd} instead of \mathcal{J}^{2nd} was found to improve

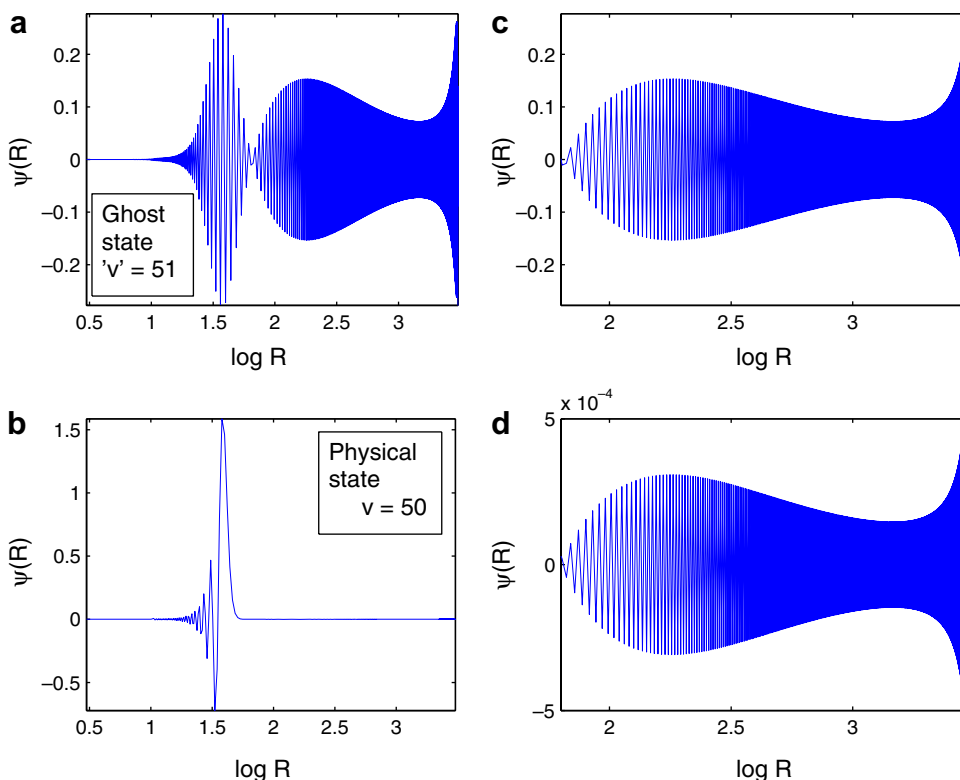


Fig. 2. (a) The wavefunction of the ghost state and (b) the adjacent physical eigenstate. (c) and (d) are a zoom-in of panels of (a) and (b).

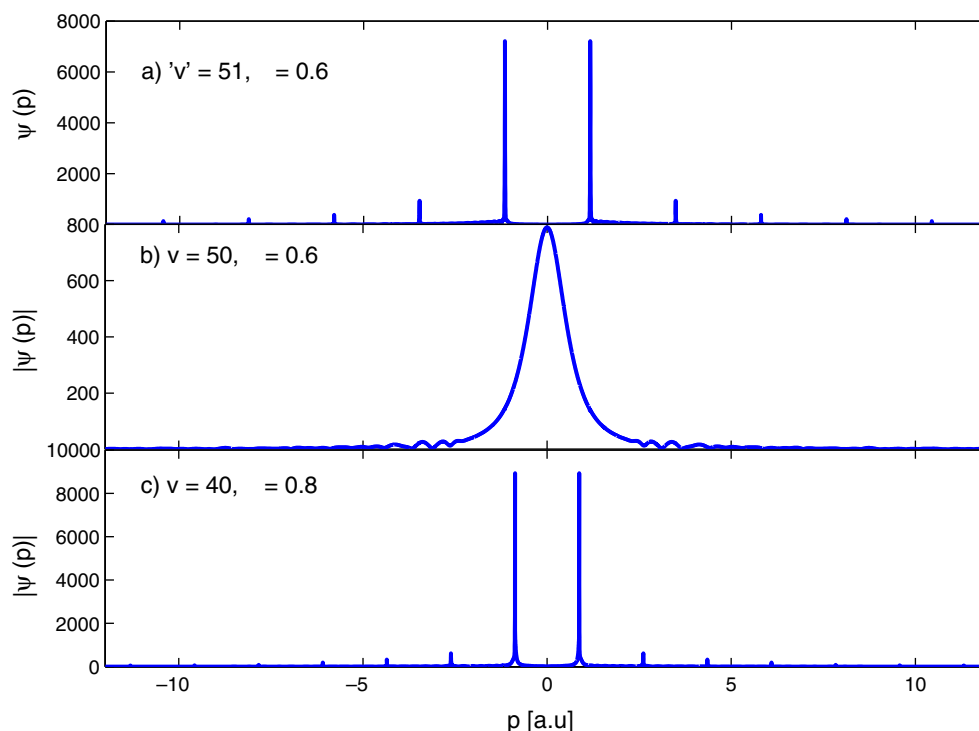


Fig. 3. (a) The wavefunction of the ghost state and (b) the closer physical eigenstate in momentum space. (c) The unphysical wavefunction in momentum space for $\beta = 0.8$.

the sampling by about 40%. For the conditions of this paper the ghosts were found to disappear for $N > 731$ points, and $\beta < 0.51$. Note, however, that for methods of different orders β is no longer a good parameter due to the different way of distributing the points. Yet, the phenomenon with its characteristic features as described above, tends to appear for this method as well.

4. Shifting the energy of the ghost by an exterior complex potential

Addition of an exterior complex potential is now suggested to eliminate the ghost states. The method of complex scaling has been used primarily for locating resonances states embedded in the continuum [12]. Within the method the potential is supplemented by an imaginary component either by a direct change of spatial variables from real to complex ones, or by adding an imaginary part to the potential, e.g., absorbing potential at the grid boundaries [13,14]. The method is also widely used for simulating scattering processes. The addition of the imaginary part the Hamiltonian operator makes it non-Hermitian.

The complex scaled Hamiltonian is chosen to have the form:

$$\hat{\mathbf{H}} = \hat{\mathbf{H}} + ia \exp[b(R - R_N)], \quad (9)$$

a and b are constants. The effective influence of the scaling is an additional absorbing/creating complex boundary conditions for $R \rightarrow \infty$ for negative/positive values of a .

We checked the dependency of the energy eigenvalues on the scaling intensity a for different values of β and sizes of grid. In all the following examples $b = 0.1 \text{ Bohr}^{-1}$.

Fig. 4 shows the change of the eigenenergies due to the scaling. Only the lowest five eigenstates that have significant imaginary eigenvalues are shown. The upper and the lower panels of the figure are for grid sizes of 3000 and 6000 Bohr, respectively. Two kinds of eigenvalues can be seen in the figure. Eigenvalues that correspond to the continuum states, i.e., $\text{Re}(E) > 0$, move toward the positive direction in both the imaginary and real axis. The eigenvalue that corresponds to the ghost state is pushed mainly into the unbound part of the spectrum. For grid size of 3000 Bohr the ghost state is not a part of the physical bound spectrum for $a = 3.2 \times 10^{-5} \text{ au}$. All the eigenvalues that correspond to bound states, are unaltered due to the scaling. Moreover, all the scattering states below the continuum state with the lowest real part that are shown in the figure are also not changed. Problems which involve dynamical calculations of scattering processes demand a correct representation of a superposition of scattering states. To perform such calculations, one will need to increase a even more and push the ghost further. For $a = 7.0 \times 10^{-5}$, the real part of the unphysical state's energy is 9.2×10^{-8} Hartree. Even for a relatively small grid size we used here, 135 scattering states up to 25 mK could be represented correctly. We remark here that for our purposes the choice of the sign of a is arbitrary. An identical calculation with negative a , i.e.,

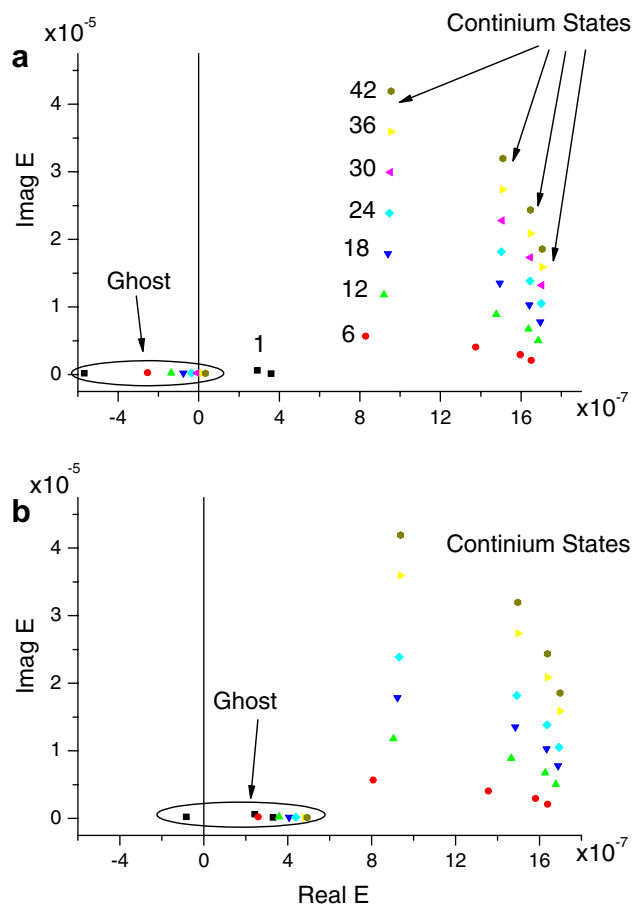


Fig. 4. (a) The effect of an addition of exterior complex potential, for various amplitudes of the exterior complex potential. The values presented in the figure are given in units of 10×10^{-6} au. Only the five eigenvalues with the lowest real energy and significant imaginary part are shown. The ghost and the continuum states are indicated. For larger amplitudes of complex potential several other energy eigenvalues moves into the complex plain with larger real energies and not shown here. $\beta = 0.6$, and $L_R = 3000$ Bohr. (b) Same as (a), with a grid size with $L_R = 6000$ Bohr.

absorbing boundary conditions, gives exactly the same results as in the previous example, except for the imaginary part of the eigenvalues, which are now negative, with the same magnitude.

The lower part of Fig. 4 presents the same energy eigenvalues for doubled grid size. The energy eigenvalues of the continuum exhibit exactly the same scaling and does not depend on the grid size. The ghost, however, moves into the unbound spectrum more rapidly.

The upper and the lower panels of Fig. 5 demonstrate the scaling of the energy eigenvalues for $\beta = 0.8$ and 0.5 , respectively. As was already noted previously, larger values of β lower the erroneous energy. Here, it is obvious that the scaling into more positive values is also suppressed, so that the scaling is not useful for too large β . The lower panel emphasizes this trend even more. For $\beta = 0.5$ no ghost state appear at all, but the scaling of the continuum states toward the positive real axis is more rapid.

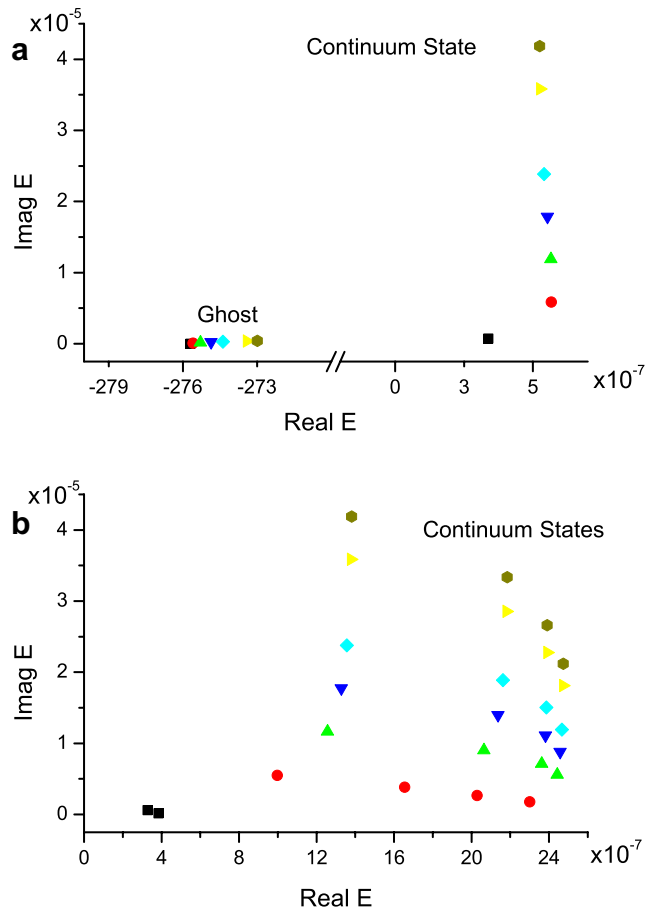


Fig. 5. (a) and (b) Same as Fig. 4(a), here for $\beta = 0.8$ and 0.5 , respectively. For $\beta = 0.8$ only the lowest continuum state is shown. The other states appear as a dense stack of levels closely to the state that is shown.

5. Discussion and summary

Understanding the origins and the characteristic features of the ghost artifact is an important step. The semi-classical method to determine the local grid spacing will create ghost states whenever the change in the potential is comparable to the local wavelength. This usually happens in high energy continuum levels of the spectrum. Imposing fixed boundary conditions as suggested by Wilner et al. [10] can eliminate some of the ghost states. An alternative high-order non-classical methods [6] forces a denser sampling in regions where the derivative of the potential is large. This improves the sampling procedure and eliminates the ghost states. As shown in this Letter, addition of an exterior complex potential can eliminate the ghost states from the bound part of the spectrum and push them, in a controllable way, to the continuum. Nevertheless, one might consider finding a way to tolerate the ghost states and account for their erroneous effects. The highly oscillatory behavior of the ghost state decouples it from all the other physical states, and allow to identify and control the error introduced.

Acknowledgements

This work was supported by the Israel Science Foundation and by the European Commission in the frame of the Cold Molecule Research Network under Contract No. HPRN-CT-2002–00290. The Fritz Haber Center is supporter by the Minerva Gesellschaft für die Forschung GmbH München, Germany.

References

- [1] Ronnie Kosloff, *J. Phys. Chem.* 92 (1988) 2087.
- [2] Ronnie Kosloff, in: R.E. Wyatt, J.Z. Zhang (Eds.), *Dynamics of Molecules and Chemical Reactions*, Marcel Dekker, 1996, p. 185.
- [3] R.G. Littlejohn, M. Cargo, T. Carrington, K.A. Mitchell, B. Poirier, *J. Chem. Phys.* 116 (2002) 8691.
- [4] Eyal Fattal, Roi Baer, Ronnie Kosloff, *Phys. Rev. E* 53 (1996) 1217.
- [5] V. Kokoouline, O. Dulieu, R. Kosloff, F. Masnou-Seeuws, *J. Chem. Phys.* 110 (1999) 9865.
- [6] M. Nest, H.-D. Meyer, *Chem. Phys. Lett.* 352 (2002) 486.
- [7] V. Kokoouline, O. Dulieu, R. Kosloff, F. Masnou-Seeuws, *Phys. Rev. A* 62 (2000) 032716.
- [8] Christiane P. Koch, Françoise Masnou-Seeuws, Ronnie Kosloff, *Phys. Rev. Lett.* 94 (2005) 193001.
- [9] P.G. Mickelson et al., *Phys. Rev. Lett.* 95 (2005) 223002.
- [10] K. Willner, O. Dulieu, F. Masnou-Seeuws, *J. Chem. Phys.* 120 (2004) 548.
- [11] R. Meyer, *J. Chem. Phys.* 52 (1970) 2053.
- [12] N. Moiseyev, *Phys. Rep.* 302 (1998) 211.
- [13] R. Kosloff, D. Kosloff, *J. Comp. Phys.* 63 (1986) 363.
- [14] J.G. Muga, J.P. Palao, B. Navarro, I.L. Egusquiza, *Phys. Rep.* 395 (2004) 357.